J|A|C|S
ARTICLES
Published on Web 08/25/2004

Dynamic NMR Study of the Mechanisms of Double, Triple, and Quadruple Proton and Deuteron Transfer in Cyclic Hydrogen Bonded Solids of Pyrazole Derivatives

Oliver Klein,[†] Francisco Aguilar-Parrilla,[‡] Juan Miguel Lopez,[§] Nadine Jagerovic,[||] José Elguero,[||] and Hans-Heinrich Limbach*[,§]

Contribution from the Institut für Chemie, Freie Universität Berlin, Takustrasse 3, D-14195 Berlin, Germany, and the Instituto de Química Médica, CSIC, Juan de la Cierva 3, E-28006 Madrid, Spain

Received February 4, 2004; E-mail: limbach@chemie.fu-berlin.de

Abstract: Using dynamic solid state ^{15}N CPMAS NMR spectroscopy (CP = cross polarization, MAS = magic angle spinning), the kinetics of the degenerate intermolecular double and quadruple proton and deuteron transfers in the cyclic dimer of ^{15}N labeled polycrystalline 3,5-diphenyl-4-bromopyrazole (DPBrP) and in the cyclic tetramer of ^{15}N labeled polycrystalline 3,5-diphenylpyrazole (DPP) have been studied in a wide temperature range at different deuterium fractions in the mobile proton sites. Rate constants were measured on a millisecond time scale by line shape analysis of the doubly ^{15}N labeled compounds, and by magnetization transfer experiments on a second timescale of the singly ^{15}N labeled compounds in order to minimize the effects of proton-driven ^{15}N spin diffusion. For DPBrP the multiple kinetic HH/HD/DD isotope effects could be directly obtained. By contrast, four rate constants k_1 to k_4 were obtained for DPP at different deuterium fractions. Whereas k_1 corresponds to the rate constant k^{HHHH} of the HHHH isotopolog, an appropriate kinetic reaction model was needed for the kinetic assignment of the other rate constants. Using the model described by Limbach, H. H.; Klein, O.; Lopez Del Amo, J. M.; Elguero, J. *Z. Phys. Chem.* **2004**, *218*, 17, a concerted quadruple proton-transfer mechanism as well as a stepwise consecutive single transfer mechanism could be excluded. By contrast, using the kinetic assignment $k_2 \approx k_3 \approx k^{HHHD} \approx k^{HDHD}$ and $k_3 \approx k^{HDDD} \approx k^{DDDD}$, the results could be explained in terms of a two-step process involving a zwitterionic intermediate. In this mechanism, each reaction step involves the concerted transfer of two hydrons, giving rise to primary kinetic HH/HD/DD isotope effects, whereas the nontransferred hydrons only contribute small secondary effects, which are not resolved experimentally. By contrast, the multiple kinetic isotope effects of the double proton transfer in DPBrP and of the triple proton proton transfer in cyclic pyrazole trimers studied previously indicate concerted transfer processes. Thus, between $n = 3$ and 4 a switch of the reaction mechanism takes place. This switch is rationalized in terms of hydrogen bond compression effects associated with the multiple proton transfers. The Arrhenius curves of all processes are nonlinear and indicate tunneling processes at low temperatures. In a preliminary analysis, they are modeled in terms of the Bell−Limbach tunneling model.

Introduction

The elucidation and the theoretical interpretation of the hydrogen/deuterium kinetic isotope effects (KIE) is very important for understanding the mechanisms of proton or hydrogen transfer reactions. KIE are, generally, largest for degenerate reactions, which are most conveniently followed by dynamic liquid and solid-state NMR spectroscopy. Usually, more than one proton is transferred, a circumstance which leads to the occurrence of multiple kinetic isotope effects (MKIE). For example, MKIE have been studied for several intra-[1] and intermolecular[2,3] double proton-transfer systems by NMR in the liquid and solid state. The data obtained have been used as input in testing dynamic MKIE theories.[4]

[†] Freie Universität Berlin, present address: Europäisches Patentamt München.
[‡] Freie Universität Berlin, present address: Schering AG, D-13342 Berlin, Germany.
[§] Freie Universität Berlin.
[||] CSIC Madrid.

(1) (a) Braun, J.; Schlabach, M.; Wehrle, B.; Köcher, M.; Vogel, E.; Limbach, H. H. *J. Am. Chem. Soc.* **1994**, *116*, 6593. (b) Braun, J.; Schwesinger, R.; Williams, P. G.; Morimoto, H.; Wemmer, D. E.; Limbach, H. H. *J. Am. Chem. Soc.* **1996**, *118*, 11 101. (c) Scherer, G.; Limbach, H. H. *J. Am. Chem. Soc.* **1994**, *116*, 1230. (d) Langer, U.; Latanowicz, L.; Hoelger, Ch.; Buntkowsky, G.; Vieth, H. M.; Limbach, H. H. *Phys. Chem. Chem. Phys.* **2001**, *3*, 1446. (e) Rumpel, H.; Limbach, H. H. *J. Am. Chem. Soc.* **1989**, *111*, 5429. (f) Schlabach, M.; Limbach, H. H.; Bunnenberg, E.; Shu, A.; Tolf, B. R.; Djerassi, C. *J. Am. Chem. Soc.* **1993**, *115*, 4554. (g) Scherer, G.; Limbach, H. H. *J. Am. Chem. Soc.* **1989**, *111*, 5946.
(2) (a) Gerritzen, D.; Limbach, H. H. *J. Am. Chem. Soc.* **1984**, *106*, 869. (b) Meschede, L.; Limbach, H. H. *J. Phys. Chem.* **1991**, *95*, 10267.
(3) (a) Meier, B. H.; Graf, F.; Ernst, R. R. *J. Chem. Phys.* **1982**, *76*, 767. (b) Stöckli, A.; Meier, B. H.; Kreis, R.; Meyer, R.; Ernst, R. R. *J. Chem. Phys.* **1990**, *93*, 1502. (c) Heuer, A.; Haeberlen, U. *J Chem. Phys.* **1991**, *95*, 4201.
(4) (a) Skinner, J. L.; Trommsdorff, H. P. *J. Chem. Phys.* **1988**, *89*, 897. (b) Meyer, R.; Ernst, R. R. *J. Chem. Phys.* **1990**, *93*, 5518. (c) Kim, Y. *J. Am. Chem. Soc.* **1996**, *118*, 1522. (d) Kim, Y. *J. Phys. Chem. A* **1998**, *102*, 3025.

10.1021/ja0493650 CCC: $27.50

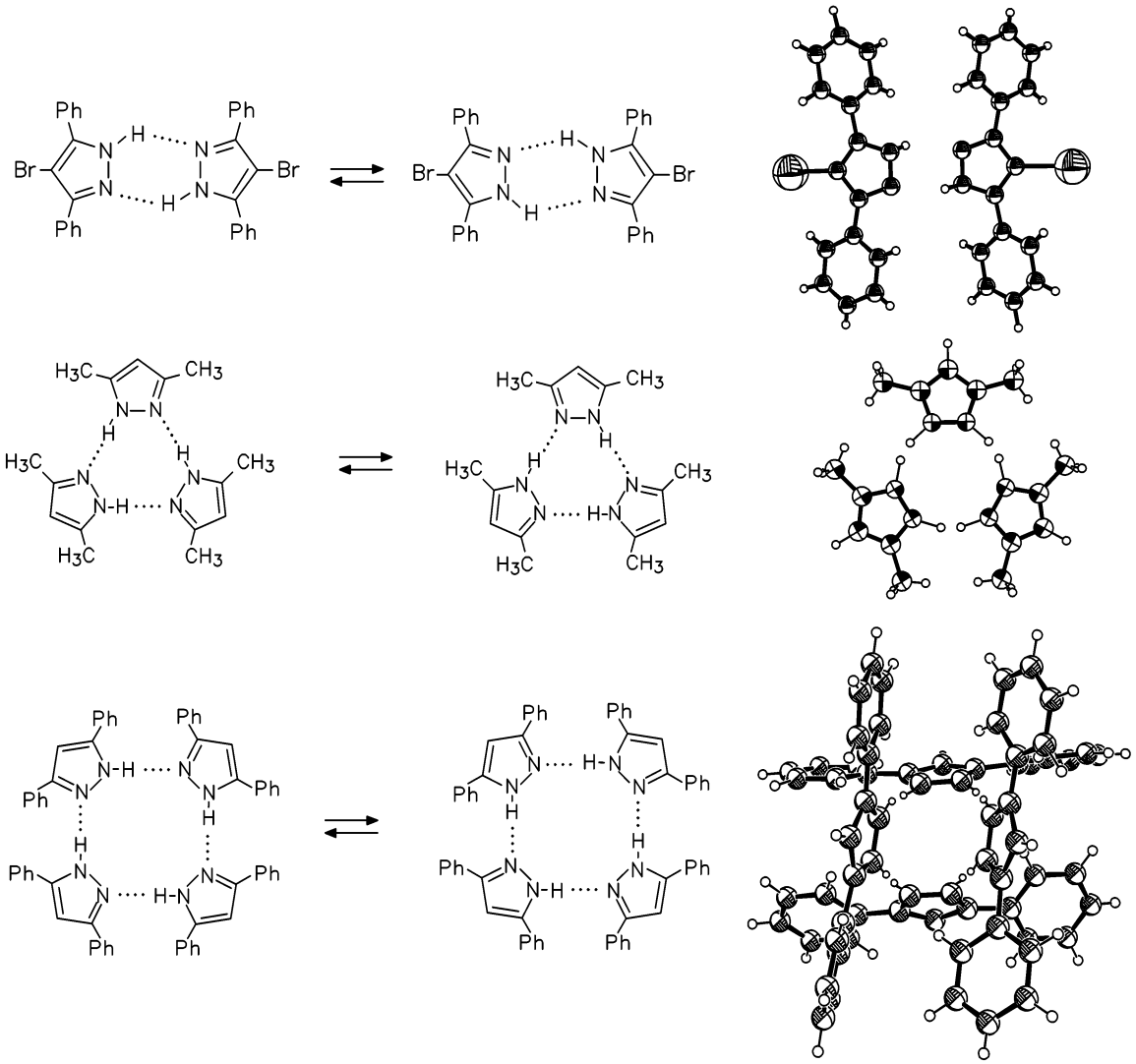

Figure 1. Intermolecular multiple proton-transfer processes in cyclic hydrogen bonded associates of pyrazoles in the solid state. (a) Cyclic dimers of 3,5-diphenyl-4-bromopyrazole (DPBrP). (b) Cyclic trimers of 3,5-dimethylpyrazole (DMP). (c) Cyclic tetramers of 3,5-diphenylpyrazole (DPP) according to ref 9. Crystal structures of DPBrP, DMP and DPP according to ref 9.

On the other hand, studies of processes in which more than two protons are transferred are rare. Horsewill et al. have reported an intramolecular quadruple proton tunneling process between the OH-groups of solid calixarene.[5] When protons are transferred from and to nitrogen, variable temperature high resolution ^{15}N CPMAS NMR (CP, cross polarization; MAS, magic angle spinning) is a very versatile method for following solid-state proton and deuteron transfers.[6] Using this method, Limbach et al. have found evidence of double proton transfers in diarylamidines.[7] Elguero et al. have studied a series of pyrazole derivatives in the solid state which can form a surprising variety of cyclic hydrogen bonded dimers, trimers, tetramers, and chains in which solid-state NMR has often detected multiple proton transfers.[8] Especially interesting was the series of pyrazole molecules depicted in Figure 1 reported several years ago:[9] in the crystalline state 3,5-diphenyl-4-bromopyrazole (DPBrP) forms cyclic dimers, 3,5-dimethylpyrazole (DMP) cyclic trimers,[8a] and 3,5-diphenylpyrazole (DPP) cyclic tetramers which exhibit degenerate double, triple and quadruple proton transfers. Ab initio calculations performed on pyrazole clusters reproduced these findings[10] and indicated a switch from concerted double and triple proton transfers to a stepwise mechanism for the quadruple transfer process, exhibiting two consecutive concerted double proton transfers. The concerted mechanism for the dimer was recently confirmed in ab initio calculations by Rauhut et al.[11]

These results motivated us to study the MKIE of these processes in more detail. Several years ago, we succeeded in measuring the full MKIE of the triple proton transfer in solid DMP[12] by dynamic variable temperature ^{15}N CPMAS NMR spectroscopy of the ^{15}N labeled compound. To our knowledge, this is the only study to date to report MKIE of a reaction in which more than two protons are transferred. The temperature-dependent kinetic HHH/HHD/HDD/DDD isotope effects could indeed be rationalized in terms of a concerted triple proton

(5) Brougham, D. F.; Caciuffo, R.; Horsewill, A. J. *Nature* **1999**, *397*, 241.
(6) Limbach, H. H. NMR—A Tool for the Study of the Dynamics of Hydrogen Transfer in Liquids and Solids. In *Encyclopedia of Nuclear Magnetic Resonance: Supplementary Volume 9: Advances in NMR*; Grant, D. M., Harris, R. K., Eds.; John Wiley & Sons, Ltd.: Chichester, 2002; pp 520−531.
(7) (a) Männle, F.; Wawer, I.; Limbach, H. H. *Chem. Phys. Lett.* **1996**, *256*, 657. (b) Anulewicz, R.; Wawer, I.; Krygowski, T. M.; Männle, F.; Limbach, H. H. *J. Am. Chem. Soc.* **1997**, *119*, 12 223.

transfer that takes place at low temperatures by tunneling. Moreover, by comparison with some additional pyrazole molecules which also form cyclic trimers in the solid state, a reduction of the barrier was observed when the size of the 3(5) substituents was reduced, an effect which could be explained in terms of a hydrogen bond compression mechanism assisting the triple proton transfer at higher temperatures.[13] Recently, some of us have used methods of formal kinetics to compute multiple kinetic H/D isotope effects of degenerate proton-transfer reactions exhibiting up to four moving protons.[14] In the quadruple proton-transfer case, various mechanisms were taken into account, i.e., a concerted quadruple proton transfer, a stepwise 2+2 and a stepwise single proton transfer. Tunneling effects[15] were described in terms of the one-dimensional Bell−Limbach[2] model. The results obtained in this study helped us to develop a strategy to elucidate, measure, and analyze these processes in the cyclic dimers of DPBrP and the cyclic tetramers of DPP.

In this paper we, therefore, report the full multiple hydrogen/deuterium isotope effects in crystalline DPBrP and DPP in a wide temperature range. For this purpose, ^{15}N CPMAS NMR experiments were performed on doubly and singly ^{15}N labeled and partially deuterated polycrystalline samples which include line shape analysis as well as magnetization transfer experiments that have been shown to provide rate constants in the millisecond to second time scale.[12] ^{15}N isotopic dilution experiments were necessary in order to exclude ^{15}N spin diffusion mediated by protons.[16]

This paper is organized as follows. After an Experimental Section, the results of the dynamic NMR experiments of MKIE in DPBrP and DPP in the solid state are presented. The results are then analyzed and interpreted.

Experimental Section

Materials. DPBrP−$^{15}N_2$ **1** and DPP−$^{15}N_2$ **2** were synthesized according to procedures reported in the literature for the unlabeled compounds,[17] starting from doubly ^{15}N labeled hydrazine sulfate. The singly labeled compounds DPBrP−^{14}N−^{15}N **3** and DPP−^{14}N−^{15}N **4** were prepared in a similar way using singly ^{15}N labeled hydrazine sulfate. The latter was synthesized starting from $^{15}NH_3$ and hydroxylamine-O-sulfonic acid.[18]

The desired deuterium fractions x_D in the mobile proton sites of **1** were achieved by mixing CH_3OD as deuterating agent and CH_3OH in the corresponding amounts under argon atmosphere, followed by evaporation of the solvent in vacuo.

^{15}N CPMAS NMR Measurements. The ^{15}N−CPMAS NMR experiments were performed using a Bruker MSL 300 spectrometer (7 T, 300.13 MHz for ^{1}H and 30.41 MHz for ^{15}N) equipped with a Chemagnetics 6 mm pencil probe. Spinning speeds were so high (5−9 kHz) that rotational sidebands could mostly be avoided. Because of sample heating in the case of the high-speed probe, a small quantity of ^{15}N labeled tetramethyltetraaza-[14]annulene (TTAA) was added to rotors in a separate capsule in order to obtain the sample temperatures from the temperature-dependent ^{15}N chemical shifts of TTAA.[19] All chemical shifts are related to external solid $^{15}NH_4Cl$ and given with an error of ±0.3 ppm. Standard CPMAS spectra were measured using the usual CP pulse sequence[20] and the line-shape analyses done as described previously.[12] The magnetization transfer experiments in the laboratory frame between the amino nitrogen magnetization S and the imino nitrogen magnetization X were performed using a sequence described previously.[16f] In these experiments, S and X are created by cross polarization and stored by 90° pulses parallel to the magnetic field B_o. The time dependence during this period is monitored after application of a second 90°pulse. The dependence is given by[16f]

$$S + X = (S_o + X_o)\exp(-\rho t),\ S - X = (S_o - X_o)\exp(-(\rho + \sigma + 2k)t) \quad (1)$$

where $\rho = 1/T_1$ represents the longitudinal relaxation rate, σ the rate of spin diffusion between S and X, and k the rate constant of the degenerate exchange between the two sites. Two experiments are performed by setting a time interval t_1 between the spin lock pulses and the 90° pulse either to 0 or to $1/2(\nu_S - \nu_X)$, where ν_S and ν_X represent the chemical shifts in Hz of the exchanging sites. In the "parallel" experiment (i) S_o and X_o have the same sign and are almost equal. Therefore, $S - X = 0$ and S and X each decay with the longitudinal relaxation rate ρ. In the "antiparallel" experiment (ii) S_o and X_o are antiparallel, i.e., $S_o \approx -X_o$, and each magnetization decays with $\rho + \sigma + 2k$ in time. As ρ is already known from experiment (i), the sum $\sigma + 2k$ is obtained in experiment (ii). Various stratagems have been proposed in order to obtain σ and k separately. Here, we exploit

(8) (a) Baldy, A.; Elguero, J.; Faure, R.; Pierrot, M.; Vicent, E. J. *J. Am. Chem. Soc.* **1985**, *107*, 5290. (b) Smith, J. A. S.; Wehrle, B.; Aguilar-Parrilla, F.; Limbach, H. H.; Foces-Foces, M. C.; Cano, F. H.; Elguero, J.; Baldy, A.; Pierrot, M.; Khurshid, M. M. T.; Larcombe-McDouall, J. B. *J. Am. Chem. Soc.* **1989**, *111*, 7304. (c) Aguilar-Parrilla, F.; Cativiela, C.; Diaz de Villegas, M. D.; Elguero, J.; Foces-Foces, M. C.; Laureiro, J. I. G.; Cano, F. H.; Limbach, H. H.; Smith, J. A. S.; Toiron, C. *J. Chem. Soc., Perkin Trans. 2* **1992**, 1737. (d) Elguero, J.; Vranzo, G. I.; Laynez, J.; Jiménez, P.; Menédez, M.; Catalán, J.; DePaz, J. L. G.; Anvia, F.; Taft, R. W. *J. Org. Chem.* **1991**, *56*, 3942. (e) Elguero, J.; Cano, F. H.; Foces-Foces, M. C.; Llamas-Saiz, A.; Limbach, H. H.; Aguilar-Parrilla, F.; Claramunt, R. M.; Lopez, C. *J. Heterocycl. Chem.* **1994**, *31*, 695. (f) Aguilar-Parrilla, F.; Männle, F.; Limbach, H. H.; Elguero, J.; Jagerovic, N. *Magn. Reson. Chem.* **1994**, *32*, 699. (g) Lamas-Saiz, A. L.; Foces-Foces, M. C.; Cano, F. H.; Elguero, J.; Jimenez, P.; Laynez, J.; Meutermans, W.; Elguero, J.; Limbach, H. H.; Aguilar-Parrilla, F. *Acta Crystallogr.* **1994**, *B50*, 746. (h) Aguilar-Parrilla, F.; Limbach, H. H.; Foces-Foces, M. C.; Cano, F. H.; Jagerovic, N.; Elguero, J. *J. Org. Chem.* **1995**, *60*, 1965. (i) Elguero, J.; Jagerovic, N.; Foces-Foces, M. C.; Cano, F. H.; Roux, M. V.; Aguilar-Parrilla, F.; Limbach, H. H. *J. Heterocyclic Chem.* **1995**, *32*, 451. (j) Lopez, C.; Claramunt, R. M.; Llamas-Saiz, A.; Foces-Foces, M. C.; Elguero, J.; Sobrados, I.; Aguilar-Parrilla, F.; Limbach, H. H. *New J. Chem.* **1996**, *20*, 523. (k) Hoelger, C.; Limbach, H. H.; Aguilar-Parrilla, F.; Elguéro, J.; Weintraub, O.; Vega, S. *J. Magn. Res.* **1996**, *A120*, 46. (l) Catalan, J.; Abboud, J. L. M.; Elguero, J. *Adv. Heterocycl. Chem.* **1987**, *41*, 187. (m) Toda, F.; Tanaka, K.; Foces-Foces, M. C.; Llamas-Saiz, A.; Limbach, H. H.; Aguilar-Parrilla, F.; Claramunt, R. M.; Lopez, C.; Elguero, J. *J. Chem. Soc. Chem. Commun.* **1993**, 1139. (n) Aguilar-Parrilla, F.; Claramunt, R. M.; Lopez, C.; Sanz, D.; Limbach, H. H.; Elguero J. *J. Phys. Chem.* **1994**, *98*, 8752. (c) Foces-Foces, C.; Echevarría, A.; Jagerovic, N.; Alkorta, Jose Elguero, I.; Langer, U.; Klein, O.; Minguet-Bonvehí, M.; Limbach, H. H. *J. Am. Chem. Soc.* **2001**, *123*, 7898.

(9) Aguilar-Parrilla, F.; Scherer, G.; Limbach, H. H.; Foces-Foces, M. C.; Cano, F. H.; Smith, J. A. S.; Toiron, C.; Elguero, J. *J. Am. Chem. Soc.* **1992**, *114*, 9657.

(10) de Paz, J. L. G.; Elguero, J.; Foces-Foces, M. C.; Llamas-Saiz, A.; Aguilar-Parrilla, F.; Klein, O.; Limbach, H. H. *J. Chem. Soc., Perkin Trans. 2* **1997**, 101.

(11) Schweiger, S.; Rauhut, G. *J. Phys. Chem. A* **2003**, *107*, 9668.

(12) Aguilar-Parrilla, F.; Klein, O.; Elguero, J.; Limbach, H. H. *Ber. Bunsen-Ges. Phys. Chem.* **1997**, *101*, 889.

(13) Klein, O.; Bonvehi, M. M.; Aguilar-Parrilla, F.; Elguero, J.; Limbach, H. H. *Israel J. Chem.* **1999**, *34*, 291.

(14) Limbach, H. H.; Klein, O.; Lopez Del Amo, J. M.; Elguero, J. *Z. Phys. Chem.* **2004**, *218*, 17.

(15) (a) Bell, R. P. *The Tunnel Effect*, 2nd ed.; Chapman and Hall: London, 1980. (b) Caldin, E.; Gold, V. *Proton Transfer*; Chapman and Hall: London, 1975. (c) Melander, L.; Saunders, W. H. *Reaction Rates of isotopic Molecules*; John Wiley & Sons: New York, Toronto, 1980.

(16) (a) Szeverenyi, N. M.; Sullivan, M. J.; Maciel, G. E. *J. Magn. Reson.* **1982**, *47*, 462. (b) Caravatti, P.; Deli, J. A.; Bodenhausen, G. R.; Ernst, R. R. *J. Am. Chem. Soc.* **1982**, *104*, 5506. (c) Linder, M.; Henrichs, P. M.; Hewitt, J. M.; Massa, D. J. *J. Chem. Phys.* **1985**, *82*, 1585. (d) Henrichs, P. M.; Linder, M.; Hewitt, J. M. *J. Chem. Phys.* **1986**, *85*, 7077. (e) Suter, D.; Ernst, R. R. *Phys. Rev. B* **1985**, *32*, 5608. (f) Limbach, H. H.; Wehrle, B.; Schlabach, M.; Kendrick, R. D.; Yannoni, C. S. *J. Magn. Reson.* **1988**, *77*, 84. (g) Robyr, P.; Meier, B. H.; Ernst, R. R. *Chem. Phys. Lett.* **1989**, *162*, 417.

(17) (a) Elguero, J.; Jacquier, R. *Bull. Soc. Chim. Fr.* **1966**, 2832. (b) Hüttel, R.; Büchele, F.; Jochum, P. *Chem. Ber.* **1955**, *88*, 1577.

(18) Bak, B.; Christensen, C. H.; Christensen, D.; Hansen, T. S.; Pedersen, E. J.; Nielsen, J. T. *Acta Chem. Scand.* **1965**, *19*, 2434.

(19) (a) Aguilar-Parrilla, F.; Wehrle, B.; Bräunling, H.; Limbach, H. H. *J. Magn. Reson.* **1990**, *87*, 592. (b) Wehrle, B.; Aguilar-Parrilla, F.; Limbach, H. H. *J. Magn. Reson.* **1990**, *87*, 584.

(20) Torchia, D. *J. Magn. Reson.* **1978**, *30*, 613.

the circumstance that σ is strongly dependent on the distance between the ^{15}N nuclei, in contrast to k. Thus, σ could be minimized by performing the magnetization transfer experiments on singly ^{15}N labeled DPBrP and ^{15}N labeled DPP instead of using the doubly labeled material.

Results

^{15}N CPMAS NMR Line Shape Analysis and Magnetization Transfer Experiments Performed on Solid DPBrP. In this section, we report the results of the dynamic ^{15}N CPMAS NMR experiments performed on polycrystalline DPBrP as a function of temperature and of the deuterium fraction x_D in the mobile proton sites. Here, we need to consider three possible isotopologs, the HH, HD-, and the DD species, whose mole fractions are given in the case of a statistic isotopic distribution by

$$x_{HH} = (1 - x_D)^2,\ x_{HD} = 2(1 - x_D)x_D,\ x_{DD} = x_D^2 \qquad (2)$$

In a first stage, ^{15}N CPMAS NMR spectra of DPBrP were measured and analyzed at $x_D = 0$ at different temperatures in order to obtain k^{HH}. Some typical results are shown in the upper left corner of Figure 2. As reported previously,[9] at low temperatures two signals are observed at 163.4 and 247.6 ppm for the amino-(−NH−, −ND−) and imino- (−N═) nitrogen atom sites. As the cross polarization and rotation frame relaxation of nuclei depend on the chemical environment, especially on the distance to the next proton,[12] one expects signal intensity distortions in the resulting spectra. However, as described previously, the cross polarization times t_{CP} used in the experiments can be adjusted in the case of polycrystalline ^{15}N labeled pyrazoles in such a way that the signals of the amino and imino nitrogen atoms sites exhibit almost equal intensities. Small differences are also averaged out by magnetization transfer arising from the tautomerism. The four sharp lines stem from the ^{15}N chemical shift thermometer TTAA added to the rotor, as mentioned in the Experimental Section, where the line positions indicate the sample temperature.

As temperature is increased, the lines broaden and coalesce, where the coalescence temperature is around room temperature for $x_D = 0$. At 308 K only one fairly sharp line is observed at $x_D = 0$. The observation that the coalesced line appears in the center of the two low-temperature signals indicates that all nitrogen atoms have an equal proton density of 0.5, i.e., that the equilibrium constant of the double proton transfer $K = 1$ is within the margin of error. The rate constants k^{HH} were determined by adapting the line shapes calculated in terms of the usual two-site reaction system to the experimental data, as indicated by the solid lines in Figure 2.

When the deuterium fraction x_D is increased, the coalescence temperature is increased, as depicted in Figure 2. Two new isotopologs can be distinguished, the HD and the DD isotopologs. The total ^{15}N NMR line shape can then be decomposed into a sum of three independent two-site reaction systems, depending on the rate constants k^{HH}, k^{HD}, and k^{DD}. As shown in the case of DMP,[12] by carefully adjusting the cross polarization times t_{cp}, it is possible to achieve a situation where line intensity distortions arising from cross polarization are minimized in such a way that the contributions of the ^{15}N−H···^{15}N and the ^{15}N−D···^{15}N hydrogen bonds of the HD species to the total line shapes are the same. ^{15}N CPMAS NMR spectra measured under these conditions at deuterium fractions $x_D > 0$ are included in Figure 2. The line shape calculations were performed assuming that all rate constants k^{LL} are independent of x_D. Thus, as k^{HH} was known from the measurements at $x_D = 0$, we only needed to vary the rate constants k^{HD}, k^{DD}. The mole fractions x_{LL} were calculated from the value of x_D according to eq 2. This value was obtained for each sample by line shape analysis of those spectra at a given temperature that provided the best resolution of the signal components of the different isotopic species. The agreement between calculated and experimental line shapes is satisfactory. Thus, we conclude that our assumption of deuterium fraction-independent rate constants is valid. The rate constants obtained by this line shape analysis are assembled in Table 1.

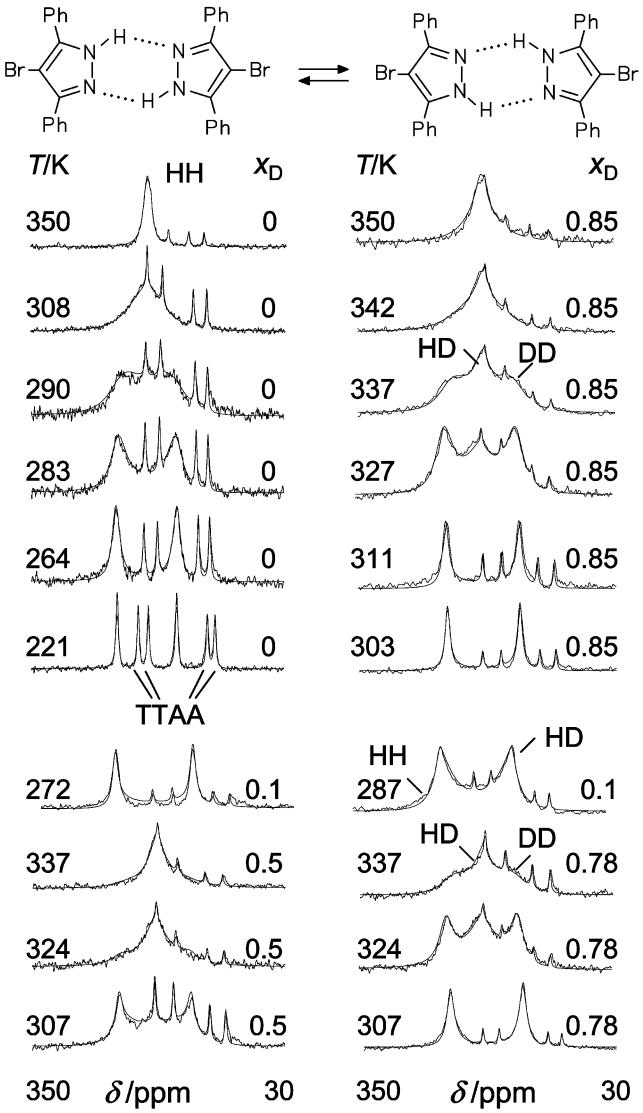

Figure 2. Superposed experimental and calculated 30.41 MHz (7 T) ^{15}N CPMAS NMR spectra of 95% ^{15}N enriched DPBrP at various deuterium fractions x_D in the mobile proton sites as a function of temperature. Experimental conditions: 5−7 kHz sample spinning, 3−12 ms CP times, 4.3 s repetition time, 5−7 μs ^{1}H 90° pulses. The four sharp lines with temperature-dependent line positions stem from a small quantity of the chemical shift thermometer ^{15}N labeled tetramethyltetraaza [14]annulene (TTAA) added in a separate capsule. The line positions directly calibrate the internal temperature of the sample inside the rotor.[19]

Since at low temperatures the reaction rates are too small to be determined accurately enough by line shape analysis, one-dimensional ^{15}N CPMAS magnetization transfers were per-

Table 1. Rate Constants of the Double Hydron Transfer in Polycrystalline DPBrP Obtained by Dynamic ^{15}N−CPMAS NMR at Various Deuterium Fractions x_D in the Mobile Hydron Sites

T/K	method	x_D	k^{HH}	k^{HD}	T/K	method	x_D	k^{HH}	k^{HD}	k^{DD}
168	MT	0.13	0.72	0.024	217	MT	0.87		0.35	0.029
179	MT	0.13	2	0.053	225	MT	0.87		1.35	0.171
196	MT	0.13	4	0.08	233	MT	0.87		4.2	0.5
215	MT	0.13	13.5	0.2	245	MT	0.87		15	1.6
225	MT	0.13	35	1.3	263	MT	0.87		80	10
230	MT	0	60		296	MT	0.87		823	192
233	MT	0.13	57	4.1	297	MT	0.87		900	225
245	MT	0.13	214	12	287	LS	0.1	2300[a]	700	
258	MT	0.13	348	50	292	LS	0.1	4000[a]	1000	
264	LS	0	480		311	LS	0.87		4000	700
272	LS	0	950		327	LS	0.87		10 000[a]	2100
283	LS	0	1900		337	LS	0.87		17 000[a]	4000
290	LS	0	3400		342	LS	0.87		20 000[a]	7000
293	LS	0	4100		350	LS	0.87		25 000[a]	8900
302	LS	0	6900		307	LS	0.5/0.8	8700[a]	3000	580
308	LS	0	9700		324	LS	0.5/0.8	2200[a]	11 000	2000
					337	LS	0.5/0.8	35 000[a]	17 000*	4000

[a] Extrapolated values used for LS. LS: ^{15}N-line shape analysis at 30.41 MHz on doubly ^{15}N labeled DPBrP. MT: magnetization transfer experiments at 30.41 MHz on singly ^{15}N labeled DPBrP. Rate constants k^{LL} in s^{-1}.

formed at low temperatures. To suppress the ^{15}N spin diffusion term σ in eq 1, we performed the following ^{15}N NMR experiments on singly (95%) ^{15}N labeled DPBrP, as previously done in the case of DMP.[12] Neglecting the spin diffusion term in eq 1, the latter can then be rewritten as

$$S + X = \sum_{LL} C_{LL} \exp(-\rho^{LL} t),$$

$$S - X = \sum_{LL} D_{LL} \exp(-(\rho^{LL} + 2k^{LL})t) \quad (3)$$

where LL refers to the numbering of the isotopologs. The coefficients C_{LL} and D_{LL} are equal to the mole fractions x_{LL} in the absence of signal intensity distortions. However, as these coefficients could be directly obtained by nonlinear least-squares fitting there was no need for an adjustment of the cross polarization times t_{CP} as in the line shape experiments.

Figure 3 shows the results of a typical experiment carried out at 30.41 MHz, 230 K and spinning speeds of about 5 to 7 kHz on singly ^{15}N labeled DPBrP. In experiment (i), not shown in Figure 3, no variation of the magnetizations within the time period covered is observed, indicating that longitudinal relaxation can be neglected. In experiment (ii), performed on the same sample under otherwise similar conditions, the two magnetizations cancel each other in the same time period because of the double proton transfer as depicted in Figure 3. A monoexponential decay of the difference between the two line intensities is observed, from which k^{HH} is obtained.

Figure 4 depicts the results of experiment (ii) performed at 217 K on a singly ^{15}N labeled DPBrP sample with $x_D = 0.87$, corresponding to statistical fractions of 0.02, 0.23, and 0.76 for the HH, HD, and DD dimers. Therefore, we assume that the HH species does not contribute to the magnetization in any significant way and can be neglected. As a consequence, a biexponential decay is observed, where the fast decay is governed by $2k^{HD}$ and the slow decay by $2k^{DD}$. Again, we note that within the margin of error the values of k^{HD} and k^{DD} do not depend on the deuterium fraction, which supports the assumption that the rate constant of double hydron transfer in a given dimer is independent of the deuterium fraction in the surrounding dimers.

^{15}N CPMAS NMR Line Shape Analysis and Magnetization Transfer Experiments Performed on Solid DPP. In the case of DPP, we have to take into account the isotopologs HHHH, HHHD, HHDD, HDHD, HDDD, and DDDD. In the case of a statistical isotopic distribution, the mole fractions of the various isotopologs are given by

$$x_{HHHH} = (1 - x_D)^4,\ x_{HHHD} = 4(1 - x_D)^3 x_D,$$

$$x_{HHDD} = 4(1 - x_D)^2 x_D^2,\ x_{HDHD} = 2(1 - x_D)^2 x_D^2$$

$$x_{HDDD} = 4(1 - x_D) x_D^3,\ x_{DDDD} = x_D^4 \quad (4)$$

Unfortunately, because of the complexity of this system, we were not able to prepare magnetizations or line shapes of the individual isotopologs and to directly determine the isotopic rate constants k^{HHHH}, k^{HHHD}, k^{HDHD}, k^{HHDD}, k^{HDDD}, k^{DDDD}. Therefore,

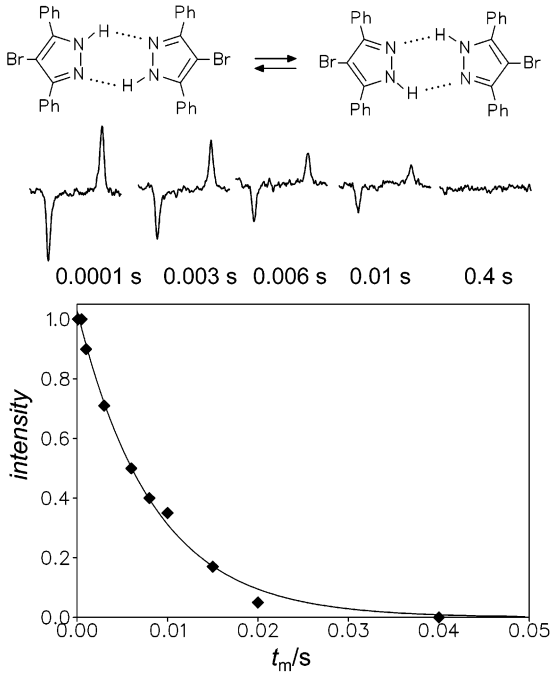

Figure 3. 30.41 MHz ^{15}N CPMAS magnetization transfer experiment in the laboratory frame performed on a sample of singly ^{15}N labeled DPBrP at 230 K and $x_D = 0$. The difference between the two magnetizations decays with twice the value of the rate constant $k^{HH} = 60\ s^{-1}$, determined by nonlinear least-squares fitting using eq 3.

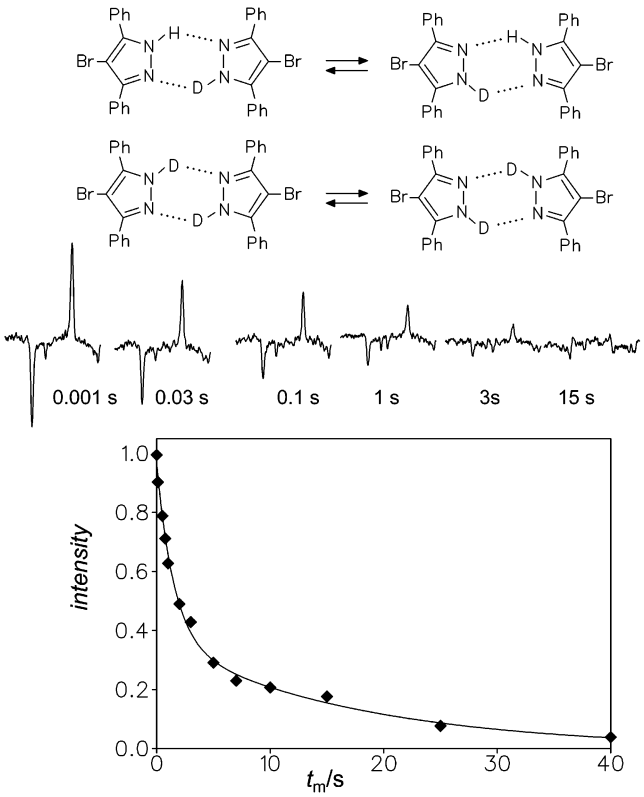

Figure 4. 30.41 MHz ^{15}N CPMAS magnetization transfer experiment in the laboratory frame performed on an undiluted sample of singly ^{15}N labeled DPBrP at 217 K and $x_D = 0.87$. The fast decay is determined by $k^{HD} = 0.35\ s^{-1}$ and the slow decay by $k^{DD} = 0.029\ s^{-1}$, determined by nonlinear least-squares fitting using eq 3.

we label the rate constants measured at different deuterium fractions k_1, k_2, ..., etc; they are shown in Table 2. Kinetic assignment, using a kinetic model presented previously,[14] will be left to the discussion.

Table 2. Rate Constants of the Quadruple Hydron Transfer in Polycrystalline DPP Obtained by Dynamic ^{15}N−CPMAS NMR at Various Deuterium Fractions x_D in the Mobile Hydron Sites

T/K	method	x_D	k_1	k_2	*T*/K	method	x_D	k_3	k_4
145	MT	0	0.003		182	MT	0.7	0.08	0.0096
169	MT	0	0.15		194	MT	0.7	0.3	0.02
180	MT	0	0.3		205	MT	0.7	0.88	0.13
190	MT	0	1.5		212	MT	0.7	2	0.25
194	MT	0	2		218	MT	0.7	2	0.4
209	MT	0	10.2		230	MT	0.7	18	3.4
222	MT	0	25		252	MT	0.7	130.5	14.52
169	MT	0.13	0.21	0.01					
184	MT	0.13	1	0.086					
194	MT	0.13	2	0.3					
204	MT	0.13	5	0.85					
220	MT	0.13	41	5					
257	LS	0	550		298	LS	>0.95		920
264	LS	0	700		303	LS	>0.95		1325
272	LS	0	1850		307	LS	>0.95		1440
278	LS	0	2500		311	LS	>0.95		2200
281	LS	0	3300		314	LS	>0.95		2800
285	LS	0	4300		320	LS	>0.95		4300
290	LS	0	6100		324	LS	>0.95		6200
292	LS	0	7200						
296	LS	0	8900						
303	LS	0	11 600						
287	LS	0.1	5050[a]	1700					
295	LS	0.1	8200[a]	3200					
304	LS	0.1	13 500[a]	5000					

[a] Extrapolated values used for LS. Rate constants k in s^{-1}. For further details, see text. LS: ^{15}N-line shape analysis at 30.41 MHz on doubly ^{15}N labeled DPP. MT: magnetization transfer experiments at 30.41 MHz on singly ^{15}N labeled DPP.

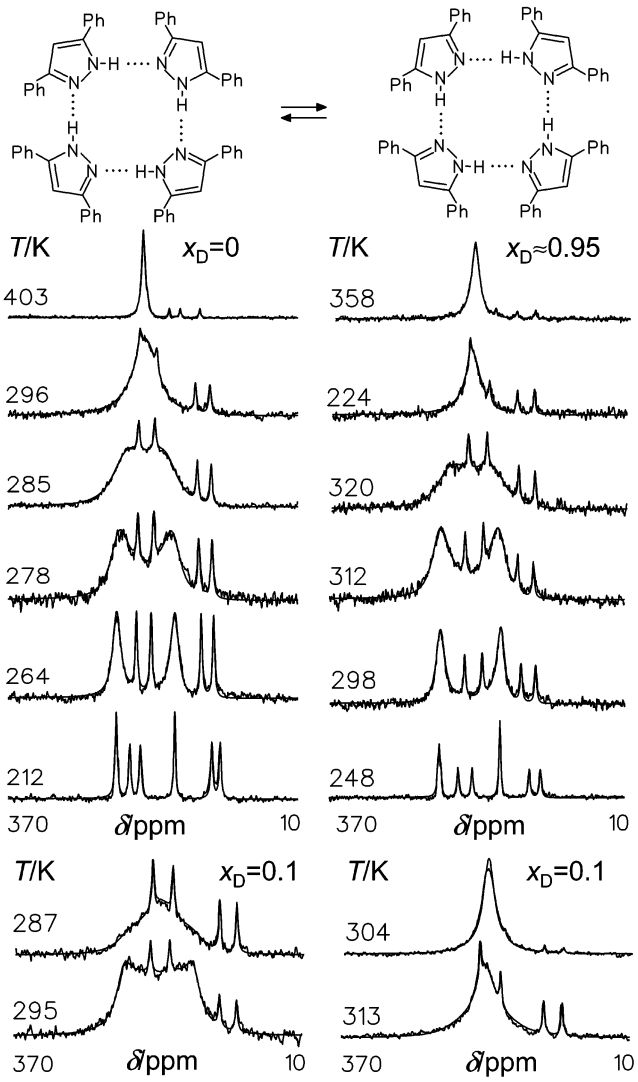

Figure 5. Superposed experimental and calculated 30.41 MHz (7 T) ^{15}N CPMAS NMR spectra of ^{15}N enriched DPP at different temperatures and deuterium fractions x_D in the mobile proton sites. Experimental conditions: 5−7 kHz sample spinning, 3−12 ms CP times, 4.3 s repetition time, 5−7 μs ^{1}H 90° pulses. The four sharp lines with temperature-dependent line positions stem from a small quantity of ^{15}N labeled tetramethyltetraaza-[14]annulene (TTAA) added in a separate capsule.

In the left upper corner of Figure 5 some typical ^{15}N CPMAS NMR spectra of DPP are depicted as a function of temperature at a deuterium fraction of $x_D = 0$. As reported above, in ref 9 at low-temperature two signals are observed at 163 and 236.1 ppm for the amino-(−NH−, −ND−) and imino- (−N═) nitrogen atom sites. The temperature dependence of the line shapes is similar to that of DPBrP, with a single centered line at high temperature, indicating a fast degenerate quadruple proton transfer, involving within the margin of error an equilibrium constant of 1. NMR cannot tell us how many protons are transferred; the number of four protons follows from the crystallographic structure. We label the rate constants obtained by line shape analysis k_1. As $x_D = 0$, this rate constant is characteristic for the HHHH isotopolog, i.e., $k_1 = k^{HHHH}$.

^{15}N CPMAS NMR spectra of a deuterated sample with a deuterium fraction of $x_D \approx 0.95$ are depicted in the upper right corner of Figure 5. In the slow exchange regime, amino and imino nitrogens exhibit intensities similar to the cross polariza-

tion times t_{CP}; for this condition to hold they had to be well-adjusted. The general line shape changes are the same as at $x_D = 0$, but the coalesence temperature has risen from 290 to 330 K. At each temperature, the line shape analysis could be performed assuming a single two-site system characterized by a single rate constant, which we label k_4. Further experiments around $x_D \approx 0.9$ did not indicate any line shape changes. This surprised us, as we expected substantial amounts of HDDD, which could have exhibited a different rate constant and hence a different line shape than the majority DDDD isotopolog.

In the next step, we measured a sample exhibiting a deuterium fraction of $x_D \approx 0.1$ (Figure 5, bottom). We used the cross polarization times t_{CP} similar to the partially deuterated samples of DPBrP in order to minimize deviations between signal intensities and mole fractions of the isotopologs. Now, to simulate the spectra, we needed to assume the presence of two superimposed two-site systems characterized by different rate constants. The rate constants of the first system coincided with k_1 within the margin of error and was assigned to the HHHH isotopolog for which we expect a mole fraction of about 0.66 according to eq 4. Therefore, we did not freely vary the k_1 values but used those extrapolated from the sample with $x_D = 0$. The second rate constant k_2 was tentatively assigned to the HHHD isotopolog exhibiting a mole fraction of about 0.29. The relative intensities of the two two-site reaction systems were taken as 0.7 and 0.3 in the temperature range covered.

To obtain rate constants at lower temperatures, we performed magnetization transfer experiments at $x_D = 0$, 0.13, and around 0.7 on singly ^{15}N-labeled polycrystalline DPP. Some results obtained at 194 K are depicted in Figures 6−8. We made sure that longitudinal relaxation did not influence the magnetizations within the time window of interest. Again, as in the case of DPBrP, the times t_{CP} were not adjusted to match magnetizations and mole fractions of the different isotopologs.

At $x_D = 0$ we obtained exponential decays, from which the rate constant $k_1 = k^{HHHH}$ could be extracted, as depicted in Figure 6. At $x_D = 0.13$, we observed a biexponential decay with amplitudes of 0.75 and 0.25, from which again two rate constants could be obtained (Figure 7). The first rate constant, $k_1 = 2\ s^{-1}$, coincided with the one obtained at $x_D = 0$ and was again assigned to the HHHH isotopolog. The second rate constant, $k_2 = 0.3\ s^{-1}$ was tentatively assigned to the HHHD isotopolog.

At $x_D = 0.7$ (Figure 8) we had expected a multiexponential decay, but in fact observed a clear a biexponential decay, characterized by two rate constants, $k_3 = 0.3\ s^{-1}$ and $k_4 = 0.02\ s^{-1}$. Our first supposition was that k_3 came from HDDD and k_4 from DDDD, but we were puzzled to observe that, within the margin of error, k_3 was equal to k_2, which made this assignment unlikely. We were able to resolve this problem only at a later stage of this study, after a thorough kinetic modeling of the quadruple proton transfer as described in the discussion.

Discussion

Using solid state ^{15}N NMR under CPMAS conditions, in particular line shape analysis and magnetization transfer experiments, we have followed the degenerate double and quadruple hydron transfer (Figure 1) in the cyclic dimers of polycrystalline

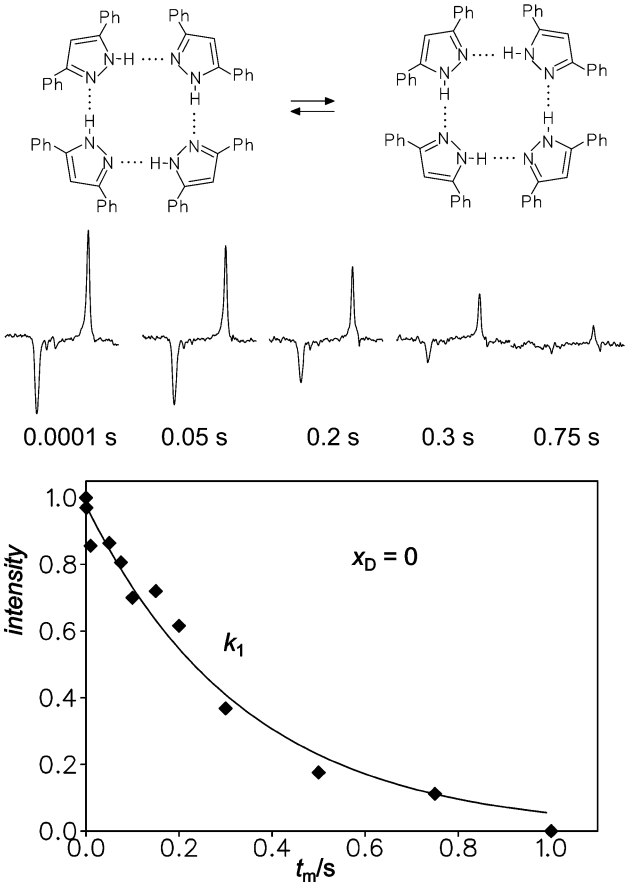

Figure 6. 30.41 MHz ^{15}N CPMAS magnetization transfer experiment in the laboratory frame performed on a sample of singly ^{15}N labeled DPP at 194 K and $x_D = 0$. The difference between the two magnetizations decays with twice the value of the rate constant $k^{HHHH} = 2\ s^{-1}$, determined by nonlinear least-squares fitting using eq 3.

singly and doubly ^{15}N labeled 3,5-diphenyl-4-bromopyrazole (DPBrP) and the cyclic tetramers of the corresponding 3,5-diphenylpyrazole (DPP) isotopologs. The multiple kinetic HH/HD/DD isotope effects of the double proton transfer could be obtained for DPBrP. For the quadruple proton transfer in DPP four rate constants k_1 to k_4 could be obtained, where k_1 corresponds to the rate constant k^{HHHH} of the HHHH isotopolog; k_2 could be tentatively assigned to k^{HHHD}, whereas the assignment of k_3 and k_4 to isotopologs had to be left open. The kinetic data obtained are plotted in the Arrhenius diagrams of Figures 9−11 as a function of the inverse temperature. We have included for comparison the Arrhenius diagram of the triple hydron transfer in solid DMP reported previously.[12] These diagrams, especially the calculated Arrhenius curves will be described and discussed below.

For a preliminary discussion we assemble in Table 3 the main kinetic parameters extrapolated for 300 K. In the case of the double proton transfer in DPBrP, we obtain at around 300 K two large single kinetic H/D isotope effects of $P_1 = k^{HH}/k^{HD} = 5$, and $P_2 = k^{HD}/k^{DD} = 5$, i.e., an overall isotope effect of $P_1P_2 = k^{HH}/k^{DD} = 25$, indicating that the "rule of the geometric mean" (RGM) is fulfilled. This leads to equally spaced Arrhenius curves of the isotopic reactions at high temperature, as illustrated in Figure 9. As has been discussed previously, this finding indicates a single-barrier mechanism, where both protons are in flight in the transition state.[2,12,14] Deviations from this rule

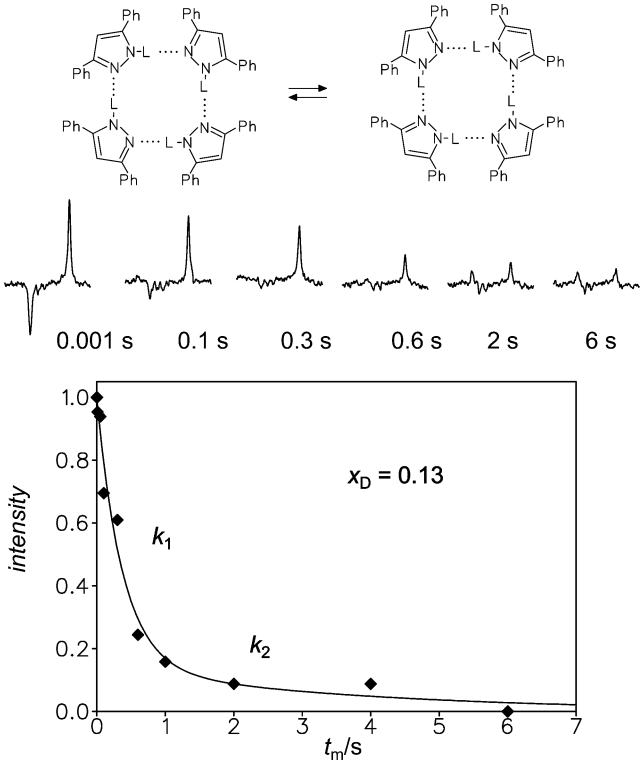

Figure 7. 30.41 MHz ^{15}N CPMAS magnetization transfer experiment in the laboratory frame performed on a sample of singly ^{15}N labeled DPP at 194 K and $x_D = 0.13$. Two rate constants, $k_1 = k^{HHHH} = 2$ s^{-1} and $k_2 = 0.3$ s^{-1}, are obtained by nonlinear least-squares fit in a similar way as in Figure 4. For the assignment of k_2, see the discussion.

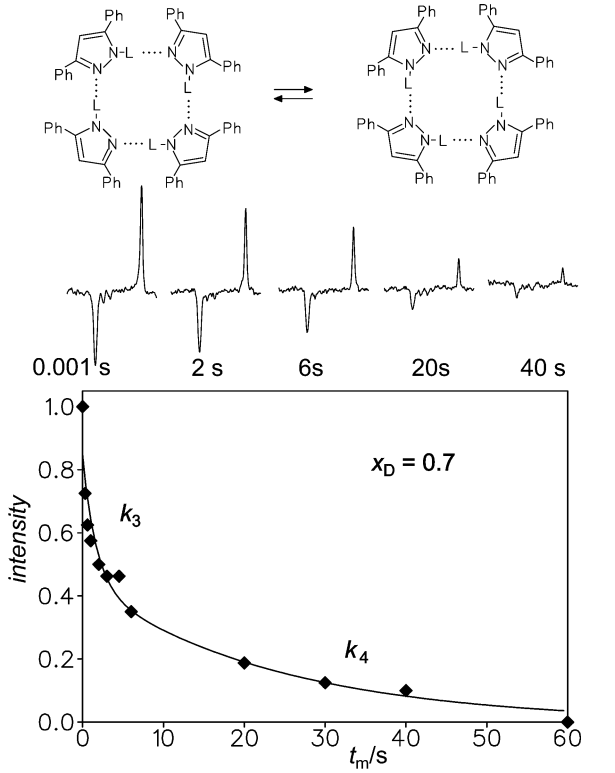

Figure 8. 30.41 MHz ^{15}N CPMAS magnetization transfer experiment in the laboratory frame performed on a sample of singly ^{15}N labeled DPP at 194 K and $x_D = 0.7$. Two rate constants, $k_2 = 0.3$ s^{-1}, and $k_3 = 0.02$ s^{-1}, are obtained by nonlinear least-squares fit in a similar way as in Figure 4, and assigned in the discussion.

arise from tunneling at low temperatures. As indicated in Table 3, this rule is also fulfilled at high temperatures for the triple proton transfer in DMP, where the Arrhenius diagram also exhibits equally spaced Arrhenius curves (Figure 10). This finding has also been discussed in terms of a single-barrier triple proton-transfer process.[12] Here, the primary kinetic single H/D isotope effects are a little bit smaller than in the case of the double proton transfer; however, the overall isotope effect has increased from 25 at 298 K for the HH transfer to 47 for the HHH transfer. If the HHHH transfer in DPP also involved a single-barrier, then we would expect a further increase in the overall isotope effect, although the single isotope effects could decrease. However, the overall isotope effect k_1/k_4 was only 12 at 298 K, whereas the first effect k_1/k_2 was already 3 (Table 3). These results indicate a change of the reaction mechanism in DPP. However, before we could elucidate the details of the changes, the rate constants k_1 to k_4 had to be kinetically assigned in terms of an appropriate kinetic model described in the following.

Multiple Kinetic Isotope Effects and Mechanisms of Degenerate Quadruple Proton Transfers. Whereas degenerate single proton transfers in the gas phase in systems of the malonaldehyde[21] or tropolone[22] type or double proton transfers in formic acid dimers[23] in the gas phase are generally coherent tunneling processes described by a tunnel frequency, they become incoherent in condensed matter, where they can be described in terms of rate constants if the barriers of proton

Table 3. Rate Constants (s^{-1}) and Kinetic Isotope Effects of the Multiple Double, Triple and Quadruple Hydron Transfers in Polycrystalline DPBrP, DMP[12], and DPP at 298 K

DPBrP				
k^{HH}	6500	k^{HH}/k^{DD}	P_1P_2	25
k^{HD}	1350	k^{HH}/k^{HD}	P_1	5
k^{DD}	260	k^{HD}/k^{DD}	P_2	5
DMP				
k^{HHH}	1016	k^{HHH}/k^{DDD}	$P_1P_2P_3$	47
k^{HHD}	270.5	k^{HHH}/k^{HHD}	P_1	3.8
k^{HDD}	73.5	k^{HHD}/k^{HDD}	P_2	3.7
k^{HDD}	21.6	k^{HDD}/k^{DDD}	P_3	3.4
DPP				
k_1	13 800	k_1/k_4		12
k_2	4000	k_1/k_2		3
k_4	1325	k_2/k_4		4

transfers are large.[24] An appropriate chemical reaction model for degenerate quadruple proton transfers has been developed recently[14] by extending models for double[1,2] and triple[12] proton transfers in organic compounds. Inspired by our previous ab initio study,[10] we considered three limiting cases, i.e., a single barrier (Figure 12a), a double barrier (Figure 12b) and a quadruple-barrier reaction path (Figure 12c). As each proton can be in two positions of the hydrogen bond, 0 and 1, we label

(21) Meyer, R.; Ha, T.-K. *Mol. Phys.* **2003**, *101*, 3263.
(22) Redington R. L.; Sams, R. L. *J. Phys. Chem. A* **2002**, *106*, 7494.
(23) Madeja, F.; Havenith, M. *J. Chem. Phys.* **2002**, *117*, 7162.
(24) (a) Firth, D. W.; Barbara, P. F.; Trommsdorf, H. P. *Chem. Phys.* **1989**, *136*, 349. (b) Horsewill, A. J.; Brougham, D. F.; Jenkinson, R. I.; McGloin, C. J.; Trommsdorff, H. P.; Johnson, M. R. *Ber. Bunsen-Ges. Phys. Chem.* **1998**, *102*, 317. (c) Neumann, M. A.; Craciun, S.; Corval, A.; Johnson, M. R.; Horsewill, A. J.; Benderskii, V. A.; Trommsdorff, H. P. *Ber. Bunsen-Ges. Phys. Chem.* **1998**, *102*, 325. (d) Loerting, T.; Liedl, K. R. *J. Am. Chem. Soc.* **1998**, *120*, 12595.

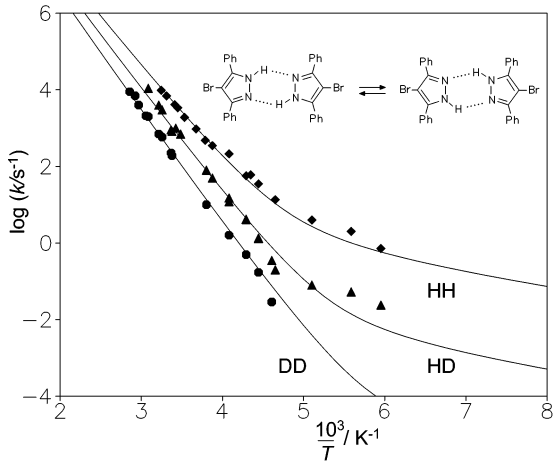

Figure 9. Arrhenius diagram for the double proton and deuteron transfer in solid DPBrP. The solid curves were calculated using the Bell−Limbach tunneling model as described in the text.

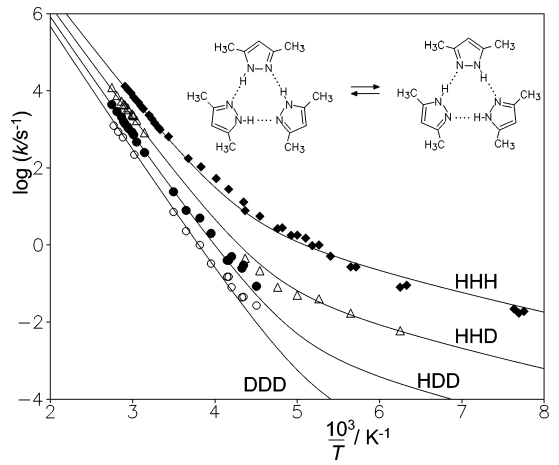

Figure 10. Arrhenius diagram for the triple proton and deuteron transfer in solid DMP. Adapted from ref 12. The solid curves were calculated using the Bell-Limbach tunneling model as described in the text.

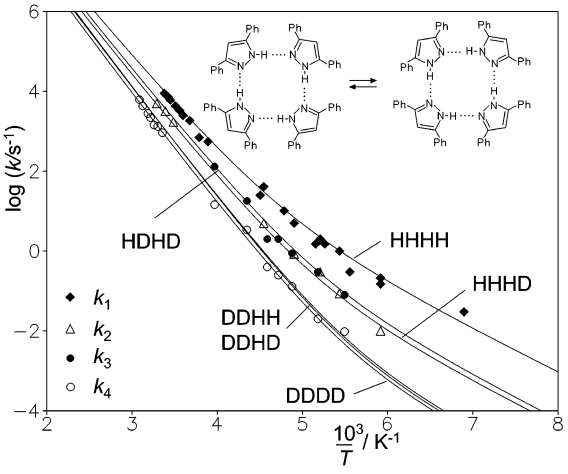

Figure 11. Arrhenius diagram for the quadruple proton and deuteron transfer in solid DPP. The solid curves were calculated using the Bell−Limbach tunneling model. For the kinetic assignment of the rate constants k_1 to k_4 to those of the calculated rate constants of the different isotopologs, see the discussion.

the two tautomers by the binary numbers 0000 and 1111. The first process does not involve any intermediate. The second process consists essentially of consecutive double proton-transfer steps, where each step involves a single barrier. There are two possibilities, either protons [1,2] are transferred first, followed by protons [3,4], or vice versa, proceeding via the zwitterionic intermediates 1100 or 0011. It is assumed that the intermediates can be treated as separate species, i.e., that there are no delocalized states involving different potential wells. This assumption will be realized when the barriers are large. Each reaction step is then characterized by an individual rate constant. The rate constant of the formation of the dissociation step is labeled k_d, and of the following neutralization step k_n. The quadruple-barrier process consists of consecutive single proton-transfer steps, corresponding to dissociation (k_d), two propagation steps (k_f and k_b), and a neutralization step (k_n). In the propagation steps one of the four protons is transferred and coupled to either a positive or to a negative charge transfer (cation or anion propagation), indicated by + or − signs. Two possible intermediates, 0101 and 1010 are double zwitterions involving very high energies, and are not considered as important.

In the following, we summarize the main results of our previous theoretical study. Secondary kinetic isotope effects were neglected in this study. In the case of the single-barrier mechanism,[14] all four hydrons are in flight in the transition state. Subsequent replacement of the H by D involves a primary kinetic isotope effect P_i, where $i = 1$ to 4:

$$k^{\mathrm{HHHD}} = k^{\mathrm{HHDH}} = k^{\mathrm{HDHH}} = k^{\mathrm{DHHH}} = P_1 k^{\mathrm{HHHH}}$$

$$k^{\mathrm{HHDD}} = k^{\mathrm{HDHD}} = k^{\mathrm{DHHD}} = k^{\mathrm{DHDH}} = k^{\mathrm{DDHH}} = P_1 P_2 k^{\mathrm{HHHH}}$$

$$k^{\mathrm{HDDD}} = k^{\mathrm{DHDD}} = k^{\mathrm{DDHD}} = k^{\mathrm{DDDH}} = P_1 P_2 P_3 k^{\mathrm{HHHH}}$$

$$k^{\mathrm{DDDD}} = P_1 P_2 P_3 P_4 k^{\mathrm{HHHH}} \tag{5}$$

For the two-barrier case, the following equations were derived[14]

$$k^{\mathrm{HHHH}} = {k_{\mathrm{d}}}^{\mathrm{HH}} \tag{6}$$

$$k^{\mathrm{HDHH}} = k_{\mathrm{d}}^{\mathrm{HH}} {P_{\mathrm{d1}}}^{-1} \frac{1 + \phi_{\mathrm{d}}}{1 + {P_{\mathrm{d1}}}^{-1} \phi_{\mathrm{d}}} \tag{7}$$

$$k^{\mathrm{DDHH}} = k_{\mathrm{d}}^{\mathrm{HH}} {P_{\mathrm{d1}}}^{-1} {P_{\mathrm{d2}}}^{-1} \frac{1 + {\phi_{\mathrm{d}}}^2}{1 + {\phi_{\mathrm{d}}}^2 {P_{\mathrm{d1}}}^{-1} {P_{\mathrm{d2}}}^{-1}} = k^{\mathrm{HHDD}} \tag{8}$$

$$k^{\mathrm{HDHD}} = k_{\mathrm{d}}^{\mathrm{HH}} {P_{\mathrm{d1}}}^{-1} \tag{9}$$

$$k^{\mathrm{HDDD}} = k_{\mathrm{d}}^{\mathrm{HH}} {P_{\mathrm{d1}}}^{-1} {P_{\mathrm{d2}}}^{-1} \frac{1 + \phi_{\mathrm{d}}}{1 + \phi_{\mathrm{d}} {P_{\mathrm{d2}}}^{-1}} \tag{10}$$

$$k^{\mathrm{DDDD}} = k_{\mathrm{d}}^{\mathrm{HH}} {P_{\mathrm{d1}}}^{-1} {P_{\mathrm{d2}}}^{-1} \tag{11}$$

where P_{d1} and P_{d2} represent the first and second primary kinetic isotope effects of the double proton transfer in the dissociation steps and ϕ_{d} the single H/D fractionation factor of

the dissociation, corresponding to the equilibrium constant of the formal reaction

$$\text{initial state (D)} + \text{intermediate state} \rightleftarrows \text{(H) initial state (H)} + \text{intermediate state (D)} \quad (12)$$

In the quadruple-barrier case we need to distinguish whether dissociation/neutralization or propagation are the rate-limiting steps. For the first case we obtained

$$k^{\mathrm{HHHH}} = 2k_{\mathrm{d}}^{\mathrm{H}} \quad (13)$$

$$k^{\mathrm{HHHD}} = \frac{1}{2}k_{\mathrm{d}}^{\mathrm{H}}[3 + P_{\mathrm{d}}^{-1}] \quad (14)$$

$$k^{\mathrm{HHDD}} = k^{\mathrm{HDHD}} = k_{\mathrm{d}}^{\mathrm{H}}[1 + P_{\mathrm{d}}^{-1}] \quad (15)$$

$$k^{\mathrm{HDDD}} = \frac{1}{2}k_{\mathrm{d}}^{\mathrm{H}}[1 + 3P_{\mathrm{d}}^{-1}] \quad (16)$$

$$k^{\mathrm{DDDD}} = 2k_{\mathrm{d}}^{\mathrm{H}}P_{\mathrm{d}}^{-1} \quad (17)$$

and for the second

$$k^{\mathrm{HHHH}} = 2k_{\mathrm{f}}^{\mathrm{H}}(1 + \alpha)K_1^{\mathrm{H}} \quad (18)$$

$$k^{\mathrm{HHHD}} = \frac{k^{\mathrm{HHHH}}}{2}\left[\frac{1 + \phi_{\mathrm{d}} + \alpha P_{\mathrm{f}}^{-1}(1 + \phi_{\mathrm{f}})}{(2 + \alpha + \alpha\phi_{\mathrm{f}}P_{\mathrm{f}}^{-1})} + \frac{\alpha(1 + \phi_{\mathrm{d}}) + P_{\mathrm{f}}^{-1}(1 + \phi_{\mathrm{f}})}{(1 + 2\alpha + \phi_{\mathrm{f}}P_{\mathrm{f}}^{-1})}\right] = k^{\mathrm{HHHD}} \quad (19)$$

$$k^{\mathrm{HHDD}} = k^{\mathrm{HHHH}}\left[\frac{P_{\mathrm{f}}^{-1}(\phi_{\mathrm{f}} + \phi_{\mathrm{d}})}{2(1 + \phi_{\mathrm{f}}P_{\mathrm{f}}^{-1})} + \frac{\phi_{\mathrm{d}} + P_{\mathrm{f}}^{-1}}{4}\right] \quad (20)$$

$$k^{\mathrm{HDHD}} = k^{\mathrm{HHHH}}\left[\frac{(P_{\mathrm{f}}^{-1} + \alpha\phi_{\mathrm{d}})(1 + \alpha\phi_{\mathrm{f}}P_{\mathrm{f}}^{-1}) + (\phi_{\mathrm{d}} + \alpha P_{\mathrm{f}}^{-1})(\phi_{\mathrm{f}}P_{\mathrm{f}}^{-1} + \alpha)}{(1 + \alpha)^2(1 + \phi_{\mathrm{f}}P_{\mathrm{f}}^{-1})}\right] \quad (21)$$

$$k^{\mathrm{HDDD}} = \frac{k^{\mathrm{HHHH}}}{2}P_{\mathrm{f}}^{-1}\left[\frac{\phi_{\mathrm{f}}P_{\mathrm{f}}^{-1}(1 + \phi_{\mathrm{d}}) + \alpha\phi_{\mathrm{d}}(\phi_{\mathrm{f}} + 1)}{(2\phi_{\mathrm{f}}P_{\mathrm{f}}^{-1} + \alpha + \alpha\phi_{\mathrm{f}}P_{\mathrm{f}}^{-1})} + \frac{\alpha\phi_{\mathrm{f}}P_{\mathrm{f}}^{-1}(1 + \phi_{\mathrm{d}}) + \phi_{\mathrm{d}}(1 + \phi_{\mathrm{f}})}{(1 + 2\alpha\phi_{\mathrm{f}}P_{\mathrm{f}}^{-1} + \phi_{\mathrm{f}}P_{\mathrm{f}}^{-1})}\right] \quad (22)$$

$$k^{\mathrm{DDDD}} = P_{\mathrm{f}}^{-1}\phi_{\mathrm{d}}k^{\mathrm{HHHH}} \quad (23)$$

Here, α constitutes a "commitment", corresponding to the ratio of the forward reaction rate constants of the anion and the cation propagation, i.e.

$$k_{\mathrm{f}}^{i-} = \alpha k_{\mathrm{f}}^{i+} = \alpha k_{\mathrm{f}}^{i} \text{ and } k_{\mathrm{b}}^{i-} = \alpha k_{\mathrm{b}}^{i+} = \alpha k_{\mathrm{b}}^{i} \quad (24)$$

where $i-$ and $i+$ are not mathematical symbols but superscripts indicating the transfer of hydron i coupled to the transfer of a negative or positive charge. K_1 represents the equilibrium constant of the dissociation step.

To visualize the above results, we assume a simple Arrhenius law for the HHHH reaction with arbitrary parameters

$$k^{\mathrm{HHHH}} = 10^{13}\exp(-27.6\ \mathrm{kJmol}^{-1}/RT) \quad (25)$$

the same preexponential factor for all isotopic reactions, and the same simple temperature dependence for all primary kinetic isotope effects

$$P = \exp(-7\ \mathrm{kJmol}^{-1}/RT) \quad (26)$$

This gives us the Arrhenius curve patterns of Figure 13. Equations 25 and 36 are valid only in a very limited temperature range, where deviations from Arrhenius laws arising from tunneling are not yet observable because of tunneling. The effects of tunneling will be included later.

In the case of the single-barrier process, we obtain five equally spaced Arrhenius curves for the different isotopic reactions, with an overall kinetic isotope effect of $k^{\mathrm{HHHH}}/k^{\mathrm{DDDD}} \approx P^4$. Generally, the transfer of n hydrons gives rise to an overall kinetic isotope effect of about P^n.[14]

In the double-barrier case (Figure 13, parts b and c), we observe three groups of Arrhenius curves, i.e., the HHHH curve, the group of the HHHD and the HDHD curves, and the group of the HHDD, HDDD, and DDDD curves. Within each group the differences are small. They are further attenuated by introducing isotope fractionation between the reactants and the intermediates, i.e.

$$\phi_{\mathrm{d}} = \exp(-0.92\ \mathrm{kJmol}^{-1}/RT) \quad (27)$$

Fractionation takes into account the fact that the zero-point energies of each proton in the intermediate are reduced due to low-frequency shifts of the proton vibrations; as a result, the differences between the rate constants of the isotopic reactions within each group are further attenuated accordingly (Figure 13c). The overall kinetic isotope effect, given by $k^{\mathrm{HHHH}}/k^{\mathrm{DDDD}} = P_{\mathrm{d}}^2$, is typical for a concerted double proton-transfer reaction. It is interesting to note that replacement of the first H by D already leads to a substantial isotope effect of $k^{\mathrm{HHHH}}/k^{\mathrm{HHHD}} = 2P_{\mathrm{d}}$.

For the four-barrier case (Figure 13d) with dissociation as rate-limiting step, an overall kinetic isotope effect of $k^{\mathrm{HHHH}}/k^{\mathrm{DDDD}} = P_{\mathrm{d}}$ is expected, typical for a single H transfer. Surprisingly, only replacement of the last H by D is affected by P_{d}. In the case of the propagation as rate-limiting step, an overall isotope effect of $k^{\mathrm{HHHH}}/k^{\mathrm{DDDD}} = P_f\phi_{\mathrm{d}}$ is expected. The isotopic rate constants lie between k^{HHHH} and k^{DDDD}. In Figure 13e, it is assumed that both cation and anion propagation exhibit the same rate constants, and in Figure 13f, it is assumed that anion propagation does not contribute fundamentally to the rate constants. This effect leads to a reduction of k^{HDHD}.

So far, we have not yet considered a specific tunneling model for each reaction step characterized by a single barrier. Our treatment, is, therefore, general and can be combined with any quantum-mechanical description referring to single-barrier processes, such as the instanton model of Smedarchina et al.,[25] which treated the stepwise double proton transfer in porphyrins in this way.

(25) Smedarchina, Z.; Zgierski, M. Z.; Siebrand, W.; Kozlowski, P. M. *J. Chem. Phys.* **1998**, *109*, 1014.

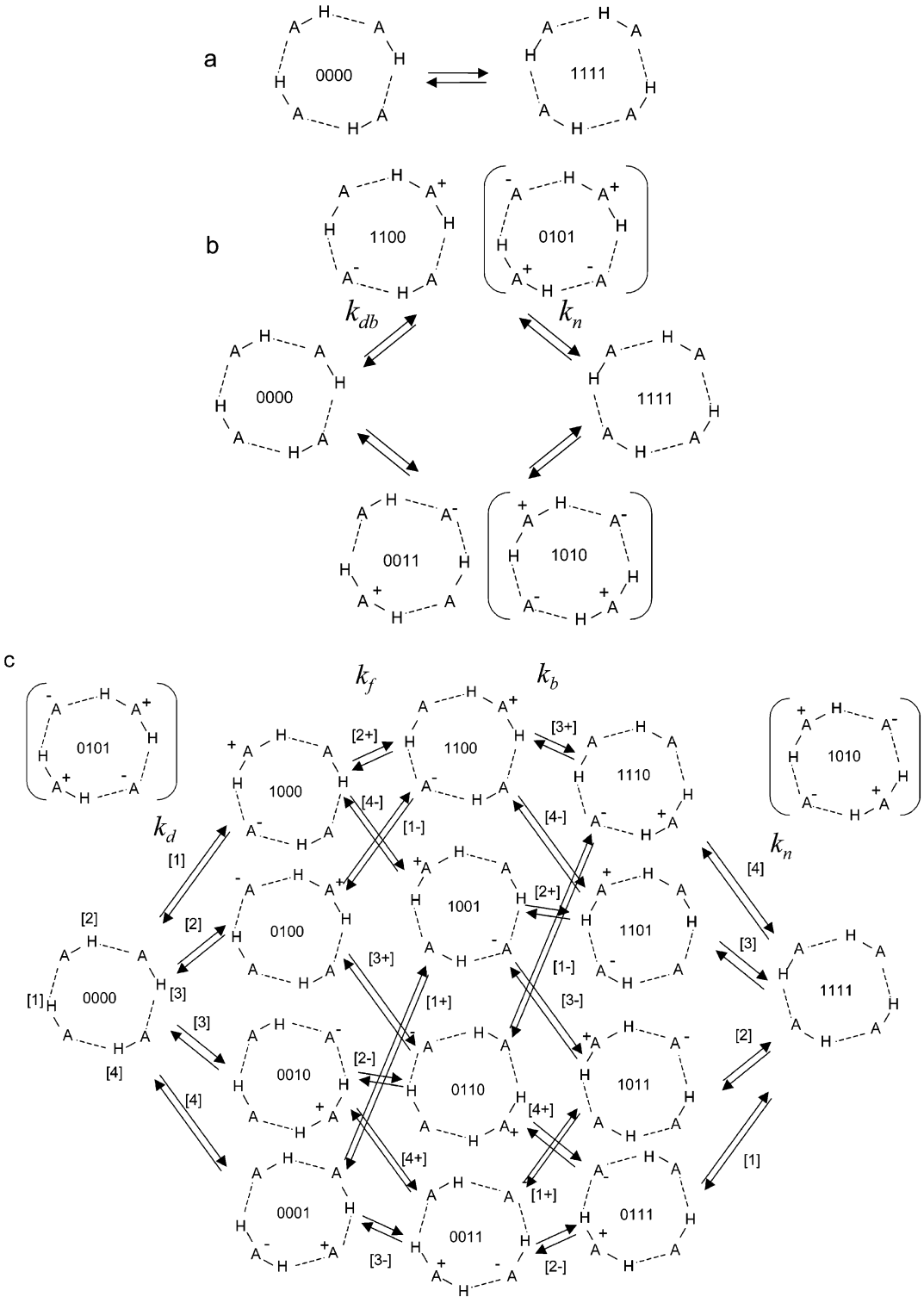

Figure 12. Single (a), double (b), and quadruple-barrier (c) mechanisms of a degenerate quadruple proton-transfer reaction.

Kinetic Assignment of the Isotopic Rate Constants of the Quadruple Proton Transfer in DPP. A comparison between the different Arrhenius curve patterns of Figure 13 and the experimental one for DPP (Figure 11) indicates that neither the single-barrier case, i.e., a concerted quadruple proton transfer, nor the quadruple-barrier cases involving single proton-transfer steps are operative in DPP. By contrast, a good agreement is obtained for the two-barrier case (Figure 13, parts b and c).

To assign the experimental rate constants k_1 to k_4 to those of the two-barrier case given by eqs 6−11, Figure 14 compares the statistical mole fractions of the various isotopic species with those of the isotopic ensembles {HHHH}, {HHHD,HDHD} and {HHDD,HDDD,DDDD}, where each ensemble is in a good approximation characterized by a single rate constant. Suddenly, we understand all the puzzling DPP results described above. The observation that the line shapes, i.e., the observed rate

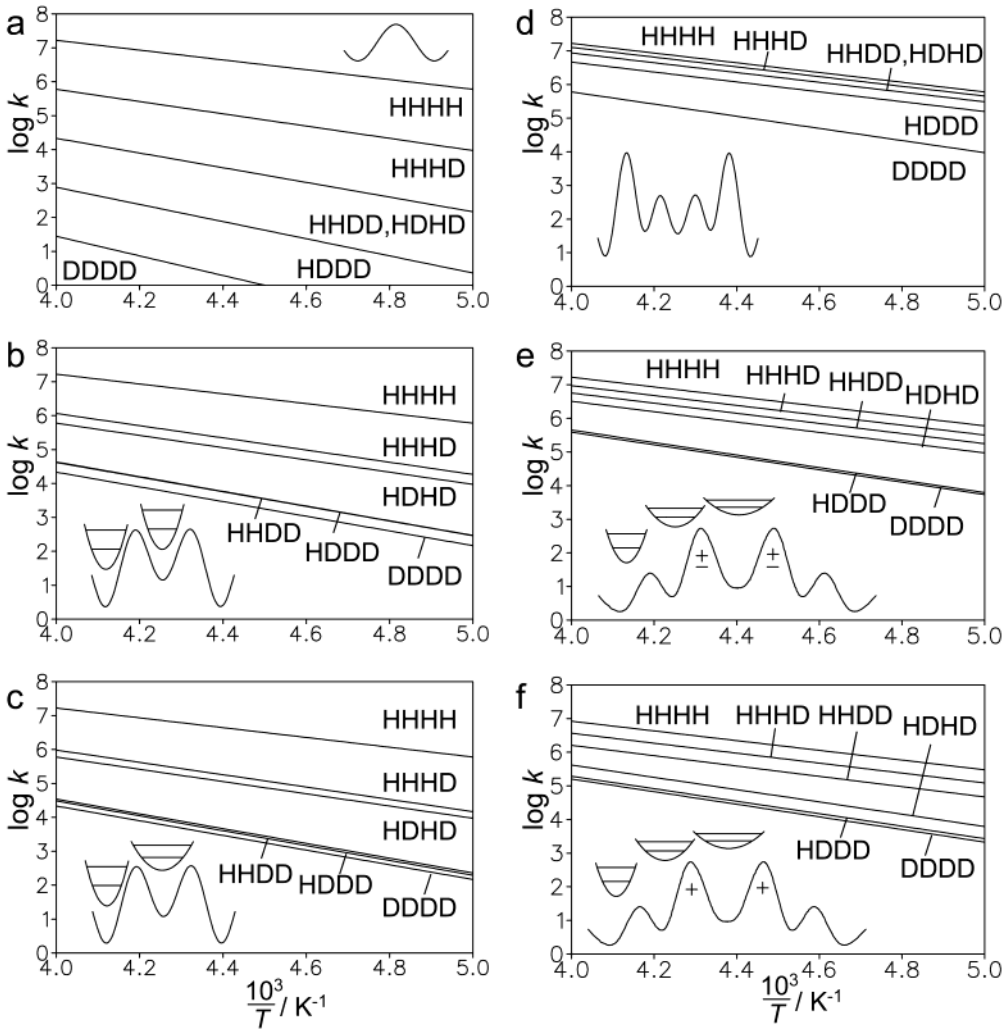

Figure 13. Simulated Arrhenius diagrams of a degenerate quadruple hydron transfer. Arrhenius laws are assumed for the HHHH transfer using the arbitrary parameters indicated in eqs 25, 26. (a) Single-barrier case. (b) Double-barrier case with $\phi_d = 1$. (c) Double-barrier case with $\phi_d = \exp(-0.92\ \text{kJ mol}^{-1}/\text{RT})$. (d) Quadruple-barrier case with dissociation as rate-limiting step. (e) Quadruple-barrier case with propagation as rate-limiting step, equal cation and anion propagation $\alpha = 1$ (as indicated by the $\pm$ signs), $\phi_d = \phi_f = \exp(-0.92\ \text{kJ mol}^{-1}/\text{RT})$. (f) Quadruple-barrier case with propagation as rate-limiting step, only cation propagation $\alpha = 0$ (as indicated by the + signs), $\phi_d = \phi_f = \exp(-0.92\ \text{kJ mol}^{-1}/\text{RT})$. Adapted from ref 14.

constants, do not vary between the deuterium fraction of 0.9 and 1 arises from the similarity of the rate constants of the HHDD, HDDD, DDDD reactions, which we can then assign to k_4. Moreover, as the HHHD and the HDHD species exhibit the same rate constant, it is not surprising to find an equivalence between k_2 measured at $x_D = 0.13$, arising from the HHHD species and to some extent from the HDHD species, and k_3 measured at $x_D = 0.7$, dominated by the HDHD species. Thus, we assign $k_2 \approx k_3$ to the ensemble {HHHD,HDHD}. The differences in the isotopic rate constant within each ensemble are so small that it cannot be resolved experimentally. This may be a sign of strong isotropic fractionation in the intermediate.

Finally, we would like to emphasize that to assign the experimental rate constants k_1 to k_4 the reaction network model of the previous section was a prerequisite. Without this model, we cannot exclude the stepwise mechanisms of Figure 12c.

One-Dimensional Energy Profiles and Tunneling. Let us summarize what we know at present about the reaction mechanisms of the three proton transfer systems. The one-dimensional reaction energy profiles of the single-barrier double proton transfer in DBrP and the triple proton transfer in DMP are schematically depicted in Figure 15. In the first case, the zero-point energies (ZPE) of two HH are reduced in the transition state, whereas in the second case the ZPE of three protons are reduced. At high temperatures, the reaction proceeds over the barrier, and at low temperatures by tunneling through the barrier.

By contrast, the reaction profile of the quadruple proton-transfer includes an intermediate of higher energy, which is reached by the transfer of two protons, as depicted in Figure 16. The most probable structure of the intermediate is the zwitterionic structure shown, which is reached by transfer of two protons in adjacent hydrogen bonds. As indicated in Figure 12b, a double zwitterionic structure is also conceivable; for this, however, one would expect a much higher energy, as suggested by our previous ab initio calculations.[10] However, we cannot distinguish the two intermediates by our kinetic measurements. The two protons in flight contribute mainly to the loss of ZPE in the transition state. The other two protons may also contribute, which would lead to secondary isotope effects, which were, however, neglected in our reaction model. The ZPE of the protons in the intermediate may be different from

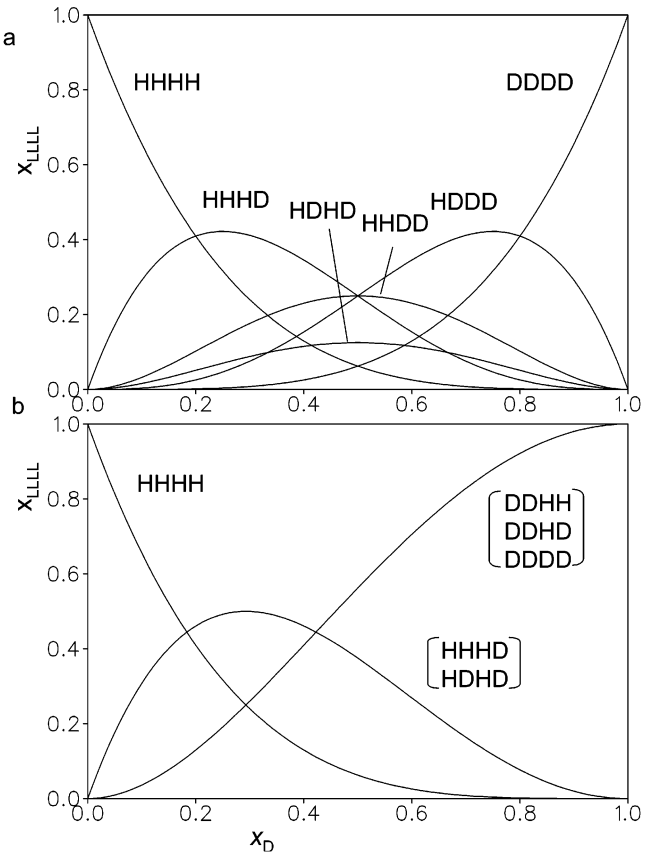

Figure 14. Mole fractions of isotopologs (a) and ensembles of isotopologs (b) of the tetrameric DPP calculated according to eq 4. For further details, see text.

those of the reactant states taken into account, which leads to isotopic fractionation between the reactant and the intermediate state.

After having established the reaction mechanisms of three processes, we come to the problem of the temperature dependence of the isotopic rate constants. We have calculated the Arrhenius curves of Figures 9−11 using a modified Bell model of tunneling, as proposed previously.[12,14] As this model is often mistaken for the original Bell model,[15] we call it the Bell−Limbach model. The main parameters of this model are as follows:

(i) $E_m = E_r + E_i$ represents a minimum energy for tunneling to occur, and is assumed to be isotope-independent. E_r represents a contribution arising from heavy atom reorganization *preceding* the hydron tunneling process at $T = 0$. E_i represents the energy of a possible intermediate and is zero in the single-barrier case.

(ii) E_d is the barrier height for the proton transfer; it does not include E_m which must be added to obtain the total barrier height.

(iii) $\Delta\epsilon$ represents the increase in the barrier height by replacing a single H with D, independent of how many H are already replaced with D. This assumption is responsible for the validity of the RGM at high temperatures.

(iv) $2a$ is the barrier width of the H transfer in Å at energy E_m.

(v) A single frequency factor A in s^{-1} is used for all isotopic reactions, i.e., a possible mass dependence is neglected within the margin of error.

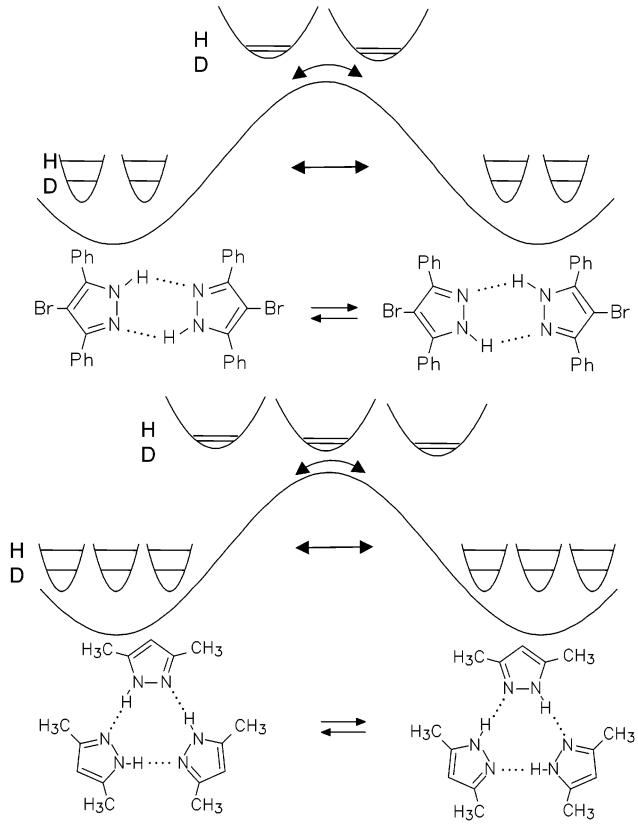

Figure 15. Reaction energy profile of the concerted double and triple proton transfer in DPBrP and DMP.

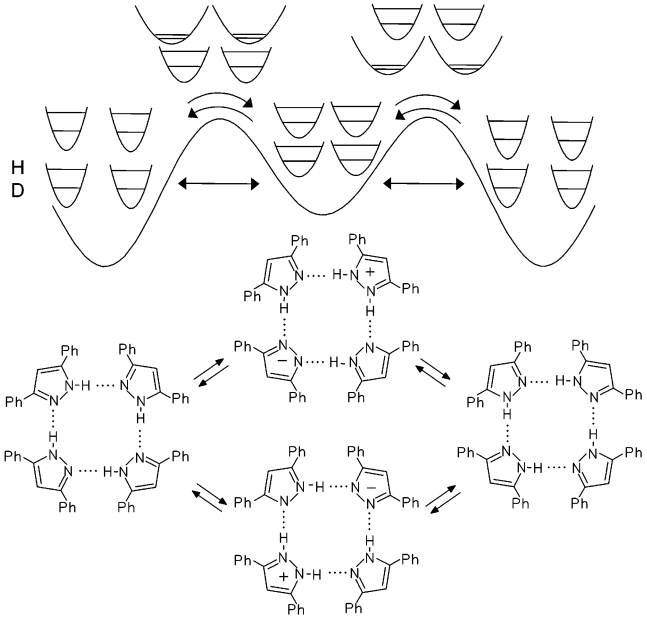

Figure 16. Reaction energy profile of the stepwise double proton transfer in DPP.

(vi) The hydron tunneling masses are increased by 1 for each H transferred, and by 2 for each D. In addition, heavy atom tunneling is taken into account by adding an additional mass Δm for each isotopic reaction. Generally, this term arises from an interconversion of double and single heavy atom bonds.

We are aware that this model is not perfect. It is only a preliminary approach to interpreting experimental Arrhenius curves until a fully quantum-mechanical description is avail-

Table 4. Parameters of the Modified Bell Model of the Double, Triple, and Quadruple Hydron Transfer in Polycrystalline 3,5-Diphenyl-4-bromopyrazole, 3,5-Dimethylpyrazole and 3,5-Diphenylpyrazole[a]

	E_d	E_m	E_d+E_m	log A	$2a$	$\Delta\epsilon$	Δm	r_{NN}/Å	r_{ND}/Å	$r_{D\cdots N}$/Å
DPBrP	47.5	5.6	53.1	12.65	0.546	3.4	2.3	2.84[8g]		
DMP	48.1	8.4	56.5	12.3	0.43	2.7	2.8	2.89[8g]	1.052[8k]	1.84[8k]
DPP	32.5	19.0	51.5	12.6	0.384	2.7	4.0	2.874[8i]	1.042[8k]	1.85[8k]

[a] Parameters of the modified Bell tunneling model used to calculate the Arrhenius curves in Figures 9 to 11. Barrier height E_d and minimum energy for tunneling E_m in kJ mol^{-1}, $\Delta\epsilon$ additional barrier energy for replacing one H by D in kJ mol^{-1}, barrier width $2a$ in Å, frequency factor A in s^{-1}. The hydron tunneling masses are 1 for each H transferred, 2 for each D. In addition, heavy atom tunneling was taken into account by adding an additional mass Δm for each isotopic reaction. For comparison, some hydrogen bond distances are also listed.

able that will provide better quantitative support for the qualitative interpretation of the Bell−Limbach model. Note that in the case of the proton exchange between acetic acid and methanol, the kinetic data were published in 1984,[2a] and a quantum-mechanical model using an instanton approach was published by Smedarchina et al. only in 2001.[26]

Table 4 lists the parameters of the Arrhenius curves of the three reactions. First, we note that the fit of the experimental data is satisfactory. The sum of the barrier height $E_d + E_m$ is fairly constant in all three compounds. E_m is of the order of 6 to 9 kJ mol^{-1} in the case of DBrP and DMP. As shown previously,[8i] there seem to be small reorientations of the pyrazoles during the proton transfer, which can be associated with E_m. In the case of DPP, this value is significantly higher; the difference of about 11 kJ mol^{-1} may arise from the energy difference between the reactant and the intermediate state. The barrier width is of the order expected given by the H-bond geometries. From the geometric data included in Table 4 a crystallographic jump distance of about 0.8 Å is expected. However, this distance refers to the two equilibrium positions of the proton in each hydrogen bond. For a zero-point stretching vibration one has to deduct twice a value of about 0.1 Å, leading to a value of about 0.6 Å, which is pretty close to the barrier widths obtained from the Arrhenius curves of DPBrP and DMP. The barrier width of DPP is further reduced because of the smaller value of E_d and the larger value of E_m as illustrated in Figures 15 and 16. The frequency factors are those expected for an intramolecular reaction. We note that the larger kinetic isotope effects of the double proton transfer in DPBrP as compared to the two other reactions is taken into account by a larger value of $\Delta\epsilon$. Finally, the heavy atom tunneling mass contribution Δm increases with the number of pyrazole molecules involved in the reaction. This finding is reasonable, as the number double bonds which are interconverted into single bonds and *vice versa* is increased.

Switch of the Reaction Mechanism from Single to Multiple Proton Transfer. In this section, we would like to discuss the observed switch of the reaction mechanism between the triple and the quadruple proton transfer. We start with a geometric hydrogen bond correlation between the two distances A····H and H····B of a hydrogen bond AHB obtained by crystallography,[27] NMR and quantum-mechanical calculations.[28] This correlation is equivalent to a correlation between the A···B distance and the deviation of the proton from the H-bond center. The shortest possible A···B distance is obtained for a symmetrical bond where H is located in the center, as visualized schematically in Figure 17a.[28] Thus, when H moves toward the center, the hydrogen bond contracts, which reduces the barrier for the H-transfer. If the energy needed for the compression is not too high, the transition state will coincide with the geometry of the symmetric hydrogen bond. Otherwise, the transition-state geometry exhibits a shorter A···B distance than in the reactant state, but a longer distance as compared to the symmetric hydrogen bond. Tunneling can take place in any configuration. Under certain conditions discussed previously, the two-dimensional problem will reduce to a one-dimensional one treated in the Bell-Limbach tunneling model.[2b,12,13]

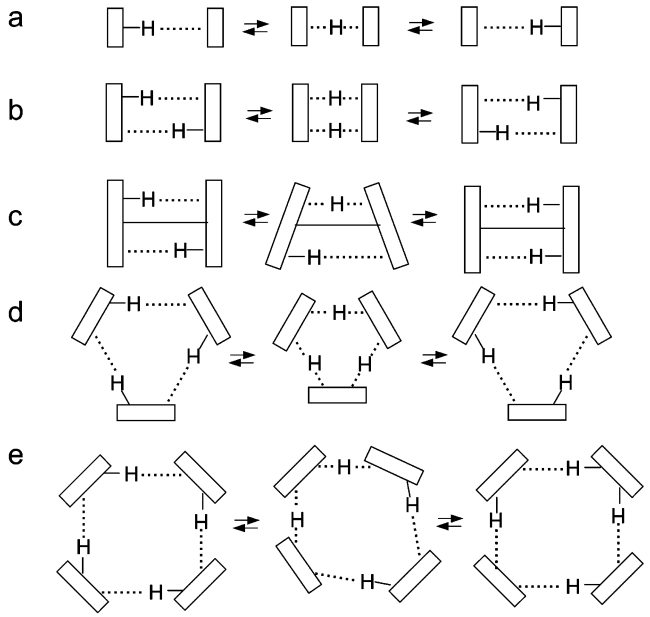

Figure 17. (a) Single proton transfer assisted by hydrogen bond compression. (b) Concerted double proton transfer assisted by the cooperative compression of two hydrogen bonds. (c) Stepwise double proton transfer in anticooperative hydrogen bonds. (d) Concerted triple proton transfer assisted by the cooperative compression of three hydrogen bonds. (e) Stepwise 2+2 quadruple proton transfer assisted by compression of two hydrogen bonds.

If two hydrogen bonds interact, then one can distinguish the cases of cooperative (Figure 17b) and of non- or anticooperative hydrogen bonds (Figure 17c). In the first case, the contraction of one hydrogen bond will lead to a contraction of the second bond. Thus, if one H is shifted toward the H-bond center and its H-bond contracts, then the second H-bond will also contract, shifting the second proton, too, to the hydrogen bond center. In other words, we obtain a concerted double proton-transfer mechanism, involving a single barrier. On the other hand, if the contraction of the first H-bond does not lead to a contraction of the second bond, or if it even leads to a widening of the latter, a stepwise proton-transfer results, involving a metastable intermediate (Figure 17c). This situation has been observed in the case of intramolecular double proton transfers, such as the tautomerism of porphyrins,[1a] azophenine,[1e] and oxalamidines.[1g]

(26) Fernández-Ramos, A.; Smedarchina, Z.; Rodríguez-Otero, J. *J. Chem. Phys.* **2001**, *114*, 1567.

(27) (a) Gilli, P.; Bertolasi, V.; Ferretti, V.; Gilli, G. *J. Am. Chem. Soc.* **1994**, *116*, 909. (b) Steiner, T.; Saenger, W. *Acta Crystallogr.* **1994**, *B50*, 348. (c) Steiner, T. *J. Chem. Soc. Chem. Commun.* **1995**, 1331. (d) Steiner, T. *J. Phys. Chem. A* **1998**, *102*, 7041.

(28) Benedict, H.; Limbach, H. H.; Wehlan, M.; Fehlhammer, W. P.; Golubev, N. S.; Janoschek, R. *J. Am. Chem. Soc.* **1998**, *120*, 2939.

As illustrated in Figure 17d, the three hydrogen bonds of DMP are cooperative, leading to a concerted triple proton-transfer involving a single barrier. A comparison of the corresponding kinetics of other cyclic trimers with more or less bulky substituents in 3,5-position were compatible with this mechanism; it was found that steric hindrance increased the barrier of the triple proton transfer.[13] If one increases the size of the hydrogen bonded system to an infinite chain, then it is clear that only a few hydrogen bonds can exhibit a cooperative coupling, as the strength of this coupling decreases with increasing distance. In such a chain, it will be impossible to compress all hydrogen bonds at the same time. This means that when some hydrogen bonds are compressed, others have to widen. At this point, we note a result reported by Eigen et al.[29] and Goodall et al.[29b] that the rate-limiting step in the neutralization of H_3O^+ and OH^- in water corresponds to a double proton transfer. In other words, one expects even for an ideal hydrogen bonded chain a switch from a concerted mechanism to a stepwise process, where in each step several H are transferred in a concerted way.

The case of DPP indicates that for cyclic pyrazoles this switch occurs between the number $n = 3$ and 4 of protons transferred, as illustrated schematically in Figure 17e. In contrast to the trimer, in the DPP tetramer it is no longer possible to compress all four hydrogen bonds at the same time.

Independently of this observed switch, it seems that the contribution of a single mobile proton site to the total kinetic isotope effect depends on the number of protons transferred, i.e., for $n = 2$, $k^H/k^D = 5$, for $n = 3$, $k^H/k^D = 3.6$, and for $n = 4$, $k^H/k^D = 3$. This dependence can be very well described by the equation $k^H/k^D = (0.96 \pm 0.11) + (8.1 \pm 0.3)\ 1/n$; for a hexamer this predicts a value of $k^H/k^D = 2.3$.

(29) (a) Eigen, M.; Kruse, W.; Maass, G.; De Maeyer, L. *Prog. Reaction Kinetics* **1964**, *2*, 285. (b) Goodall, D. M.; Greenhow, R. C.; Knight, B.; Holzwarth, J. F.; Frisch, W. *Techniques and Applications of Fast Reactions in Solutions*; Gettins, W. J., Wyn-Jones, E., Eds.; D. Reidel Publishing Company: 1979; pp 561−568.

Conclusions

The multiple kinetic hydrogen/deuterium isotope effects of a double proton-transfer reaction have been measured in the case of 3,5-diphenyl-4-bromopyrazole (DPBrP), and the multiple kinetic isotope effects of the quadruple proton-transfer reaction in the case of 3,5-diphenylpyrazole (DPP) using variable temperature solid-state NMR methods. For DPBrP, the results could be modeled with a single-barrier process involving a strong hydrogen bond compression in the transition state, and a concerted double proton tunneling process at low temperatures. In the case of DPP, the kinetic data were assigned to a stepwise quadruple proton-transfer mechanism where two protons are in flight in the rate-limiting step.

The isotope effects were described theoretically using the Bell−Limbach tunneling model. In the future, it would be desirable to apply multidimensional tunneling models in connection with ab initio calculations to this kind of reaction. In other words, the data obtained here could serve to test improved theoretical models of proton transfer.

Acknowledgment. This work has been supported by the Deutsche Forschungsgemeinschaft and the Fonds der Chemischen Industrie, Frankfurt.

JA0493650